Pertanika J. Sci. & Technol. 32 (S2): 91 - 113 (2024)

PERTANIKA JOURNALS

SCIENCE & TECHNOLOGY

Journal homepage: http://www.pertanika.upm.edu.my/

Mechanical Properties of Thermoplastic Cassava Starch/ Coconut Fibre Composites: Effect of Fibre Size

Ridhwan Jumaidin[1]*, Ainin Sofiya Gazari[1], Zatil Hafila Kamaruddin[2,3], Zatil Hazrati Kamaruddin[3], Nazri Huzaimi Zakaria[1], Syahibudil Ikhwan Abdul Kudus[1], Mohd Shukri Yob[2], Fudhail Abd Munir[4] and Meysam Keshavarz[5]

[1]Fakulti Teknologi dan Kejuruteraan Industri dan Pembuatan, Universiti Teknikal Malaysia Melaka, Hang Tuah Jaya, 76100 Durian Tunggal, Melaka, Malaysia

[2]Fakulti Teknologi dan Kejuruteraan Mekanikal, Universiti Teknikal Malaysia Melaka, Hang Tuah Jaya, 76100 Mel76100 Durian Tunggal Melaka, Malaysia

[3]German-Malaysian Institute, Jalan Ilmiah Taman Universiti, Kajang 43000, Malaysia

[4]Department of Mechanical Engineering, Faculty of Engineering, Universiti Teknologi PETRONAS, 32610 Seri Iskandar Perak Malaysia

[5]The Hamlyn Centre, Institute of Global Health Innovation, Imperial College London, Bessemer Building, South Kensington Campus, Exhibition Road, London, SW7 2AZ, United Kingdom

ABSTRACT

This research aims to study the thermal and mechanical properties of biodegradable thermoplastic cassava starch (TPCS) reinforced with various sizes of coconut husk fibre (CHF). The range of fibre sizes used was 125, 200, and 300 µm. These CHFs were integrated into a thermoplastic cassava starch matrix to make bio-composites. After integrating all components, the bio-composites were hot-pressed at 155°C for 60 minutes to produce thermoplastic sheets. Tensile and flexural tests were carried out to examine the mechanical characteristics of TPCS/CHF composites. The samples were also characterised using Thermogravimetric Analysis (TGA), X-ray diffraction (XRD), Fourier Transform Infrared Spectroscopy (FTIR), and Scanning Electron Microscopy (SEM). The findings demonstrated that a smaller 125 µm CHF improved the mechanical properties higher than other fibre sizes. Fibre with 300 µm showed more voids, which led to lower material strength. TGA results showed that 300 µm fibres enhanced the crystallinity and thermal stability of the material. FTIR and TGA showed that CHF incorporation

ARTICLE INFO

Article history:
Received: 16 August 2023
Accepted: 09 May 2024
Published: 14 June 2024

DOI: https://doi.org/10.47836/pjst.32.S2.07

E-mail addresses:
ridhwan@utem.edu.my (Ridhwan Jumaidin)
aininsof@gmail.com (Ainin Sofiya Gazari)
zatilhafila@gmail.com (Zatil Hafila Kamaruddin)
hazrati88@gmail.com (Zatil Hazrati Kamaruddin)
nazrihuzaimi@utem.edu.my (Nazri Huzaimi Zakaria)
syahibudil@utem.edu.my (Syahibudil Ikhwan Abdul Kudus)
mshukriy@utem.edu.my (Mohd Shukri Yob)
fudhail.munir@utp.edu.my (Fudhail Abd Munir)
keshavarz.meysam@gmail.com (Meysam Keshavarz)
* Corresponding author

ISSN: 0128-7680
e-ISSN: 2231-8526

© Universiti Putra Malaysia Press

increased intermolecular interactions and thermal stability. Overall, a smaller fibre size of 125 μm showed a better reinforcement effect than the larger fibre sizes, which enhanced the materials' tensile and flexural properties. This study demonstrated that modified TPCS/CHF has shown enhanced functionality than neat TPCS.

Keywords: Cassava starch, coconut husk fibre, fibre size, thermoplastic starch

INTRODUCTION

Plastic trash and pollution are pervasive across the water (oceans, rivers, lakes), land (soils, sediments, animal biomass), and air (atmosphere) (Hazrol et al., 2021; Madhumitha et al., 2018; Syafiq et al., 2020). As environmental impediments, e.g., non-biodegradable and plant wastes, as well as mounting garbage mountains, are documented, current environmental challenges become more apparent (Ilyas et al., 2022; Pradeep et al., 2022). There are limited disposal spaces and expanding incineration capacity that necessitate substantial capital expenditures and increased environmental dangers. These issues have influenced the design and development of ecologically sustainable and renewable materials as alternatives to non-biodegradable materials (Ilyas & Sapuan, 2020b, 2020a). Packaging is crucial in preserving food quality and controlling the interaction between food and the environment. It is vital to produce biodegradable packaging to prevent recycling and environmental pollution challenges caused by synthetic plastics.

Estrada-Monje et al. (2021) state that starches are crucial raw ingredients for generating bio-based blends and composites. Also, they are natural, and numerous biopolymers come from grains, e.g., cassava, maise, rice, and potato. The amylose and amylopectin contents in starch vary depending on their sources. The bioplastics' tensile properties improved as the materials' amylose content increased (Ceseracciu et al., 2015; Marichelvam et al., 2019). Starch, among the most significant industrial raw materials, is a versatile substance with a variety of applications. According to Tharanathan (2005), starch is the most common hydrocolloid in the food business, providing various functional qualities.

Thermoplastic starch (TPS) is a native starch-derived biopolymer following its granular structure modification that uses a plasticiser, such as water, glycerol, and sorbitol, among many others (Rivadeneira-Velasco et al., 2021; Mina et al., 2009). Another statement by Weerapoprasit and Prachayawarakorn (2019) is that glycerol is the ideal plasticiser for making TPS because it breaks starch granules and forms an amorphous structure. Studies have been done by Mo et al. (2010) employing thermoplastic cassava starch and reported cellulose fibre demonstrating changes in the thermoplastic starch that enhanced the material's characteristics. Hot compression moulding was used to treat the starch, plasticiser, and fibre reinforcement to make this TPS material (Jumaidin et al., 2021; Zhang et al., 2014). Furthermore, starch plays a crucial role in bio-composite structures as a matrix

or resin during the production of biopolymers. Over the years, researchers have explored various types of natural starch, including corn, sugar palm, *Dioscorea hispida*, cassava, and many others. Table 1 illustrates the utilisation of cassava starch as a thermoplastic material in bio-composites and their potential applications.

Table 1
Thermoplastic cassava starch composites and their potential applications

Thermoplastic starch blends	Potential application	Reference
Thermoplastic cassava starch/kraft	Biodegradable tray	Campos et al., 2018
Thermoplastic cassava starch/cassava bagasse	Food packaging plastic	Travalini et al., 2019
Thermoplastic cassava starch/cogon grass	Biodegradable tray	Jumaidin et al., 2020
Thermoplastic cassava starch/*Cymbopogan citratus*	Biodegradable material	Kamaruddin et al., 2022

Malaysia produces abundant agricultural waste materials, including rice husk, coconut, and oil palm frond fibre. Around 25 % of the nut is made up of coir, a challenging and rigid lignocellulosic fibre obtained from the fibrous mesocarp part of coconut fruits, as shown in Figure 1. Due to their high lignin concentration, coir fibres are resilient, weather-resistant, somewhat waterproof, and may be chemically altered. The fibres also have a high elongation at break, allowing for stretching over their elastic limit without rupturing. Among the benefits of these fibres are that they are renewable, nonabrasive, inexpensive, plentiful, and pose fewer health and safety risks during handling and processing (Abdullah et al., 2011). According to Jusoh et al. (2021), coconut fibres possess the maximum toughness of all-natural fibres. Hence, further research and development of these materials to generate the most recent polymer sources include using fibre as an amplifier in polymer composites.

Figure 1. Coconut husk

It is evident from the literature that a few research have been published on cassava starch development and the effect size of CHF. Thus, the main objective of this work is to evaluate the mechanical and thermal properties of the influence of fibre size on biodegradable thermoplastic cassava starch reinforced with coconut husk fibre composite.

MATERIALS AND METHODS

Materials

Antik Sempurna Sdn. Bhd. Malaysia supplies the cassava starch. The plasticiser in this study was glycerol purchased from QReC (Asia) Sdn. Bhd., while palm wax was acquired

from Green & Natural Industries Sdn. Bhd. (Selangor, Malaysia). Coconut husk fibre was supplied from Negeri Sembilan, Malaysia. The husk and shell were separated from the coconut by hand. Coconut fibre was prepared by crushing the long coconut fibres (Figure 2). Shredded coconut fibre was sieved and retained using 125, 200, and 300 µm circular stainless steel sievers.

Figure 2. Coconut husk fibre

Preparation of Samples

Thermoplastic cassava starch (TPCS), glycerol, palm wax, and CHF were weighed according to the (%) ratio. Before pre-mixing the TPCS samples, glycerol, palm wax, and CHF were added to a dry mixer at 120 rpm for 5 min at room temperature. The resultant mixture was then thermo-pressed at 155°C for 60 min using a Plastic Hydraulic Moulding Press under 10 tonnes to create 3 mm thick sheets. Before the conditioning, samples were immediately put in a silica gel-filled desiccator to prevent undesired moisture absorption. Thermoplastic cassava starch with palm wax and coconut husk fibre prepared earlier was kept in an airtight container to prevent it from absorbing moisture from the surrounding environment. The integration of coconut husk fibre in this portion was determined by the fibre sizes of 125, 200, and 300 µm. The process flow is shown in Figure 3.

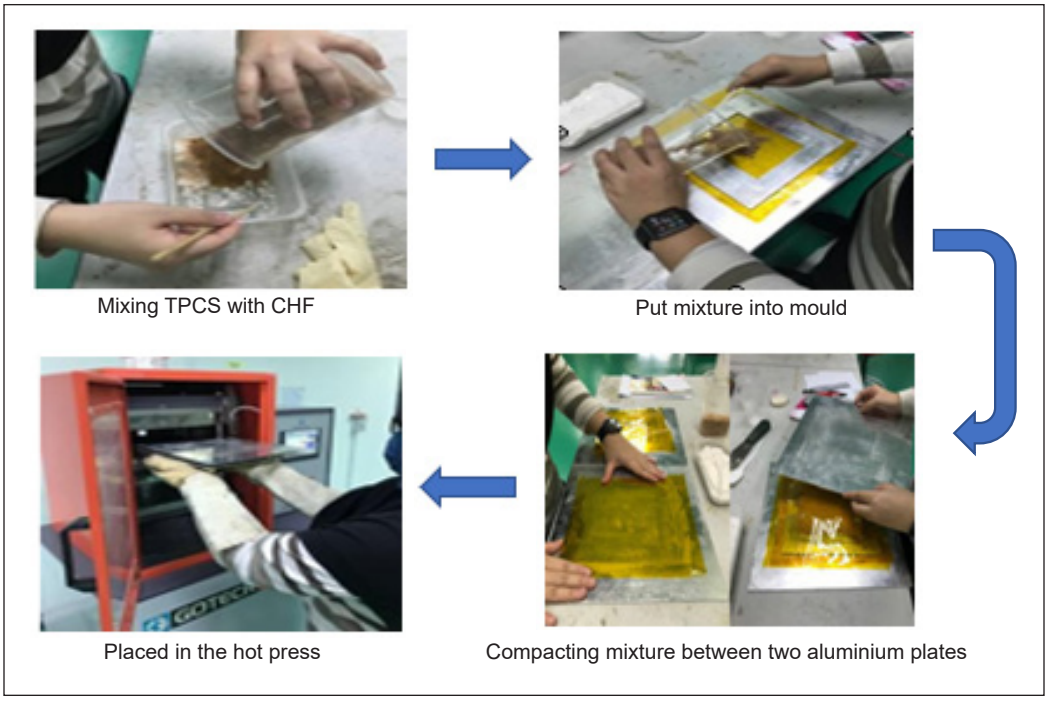

Figure 3. Fabrication of TPCS-reinforced coconut husk fibre

Tensile Testing

The tensile strength, strain, and modulus were determined using tensile testing. This test measures the required force to fracture the specimen and its length. Referencing ASTM D638 as a standard, the specimens were used to draw five samples. The samples were examined using an INSTRON 5969 Universal Testing Machine (United States) with a 5 mm/min crosshead speed of a 50 kN load cell. In addition, this test was conducted at a temperature of 24.0°C and relative humidity (RH) of 50%. The results of the tensile properties were determined by calculating the data mean.

Flexural Testing

Flexural tests were performed according to ASTM D790 at a relative humidity (RH) of 50 ± 5 % and a temperature of 23 ± 1°C. Five (5) samples with dimensions of 130 mm (L) × 13 mm (W) × 3 mm (T) each were produced. A Universal Testing Machine (INSTRON 5969) from INSTRON (United States) with a 2 mm/min crosshead speed and a 50 kN load cell was employed during the testing.

Thermo-gravimetric Analysis (TGA)

A thermogravimetric evaluation of the material's deterioration and stability was conducted. TGA was conducted using a Q-series thermal analysis instrument, namely the Mettler-Toledo AG, Analytical (Switzerland), to examine the thermal stability of the samples. The study was conducted in aluminium pans at 10°C min^{-1} at temperatures ranging from 25 to 900°C in a nitrogen environment with dynamic pressure. The weight of the sample was around 102 mg.

Fourier Transform Infrared (FT-IR) Spectroscopy

The FT-IR test assessed whether coconut husk fibre contains functional groups. This test is to determine the material's functional group and chemical characteristics. An IR spectrometer was used to get the material's spectrum (JASCO FTIR-6100 Spectrometer (Japan)). A sample of FT-IR spectra was gathered between 4000 and 500 cm^{-1}. The material was mixed with potassium bromide (KBr) to make a 1 mm thick disc weighing 2 mg in powder form.

Scanning Electron Microscope (SEM)

The morphological traits of fractured tensile samples were observed under a scanning electron microscope (SEM), Zeiss Evo 18 Research (Jena, Germany), at the pre-set 10 kV acceleration voltage. The samples were reduced to comparable sizes, and gold coating was applied to their surfaces before the observation. The tensile-analysed specimens were saved in zip-locked packing containers and characterised through SEM.

X-ray Diffraction (XRD)

The structure of the coconut husk fibre solid waste was assessed using an X-ray diffractometer (APD 2000, Italy) with Cu K-α radiation at 0.15406 nm, 40 kV, and 30 mA of wavelength, voltage, and current, respectively. The samples underwent scanning at a rate of 2° min^{-1} at room temperature across the diffraction angle range of 2θ = 5 to 60°. The crystallinity index calculation of the samples CI (%) was done referring to Equation 1:

$$CI = \frac{I - am}{I} \times 100\% CI = \frac{I - am}{I} \times 100\% \quad (1)$$

where crystalline (I) and amorphous (am) are the total area under the crystalline peaks and the amorphous halo, respectively.

Statistical Analysis

The mechanical characteristics were analysed statistically using a one-way analysis of variance (ANOVA). Using Duncan's multiple range tests, the significance of each mean property value was determined ($p<0.05$). This test was used to measure the significance of the difference between the two groups.,

RESULT AND DISCUSSION

Tensile Testing

Figure 4 depicts the tensile strength of TPCS/CHF composites for fibre sizes of 125, 200, and 300 µm. The tensile strength for size ranges of 125, 200, and 300 µm were 6.5, 4.1, and 2.3 MPa, respectively. The results have shown increments with the use of CHF reinforcement substantially in tensile strength with the addition of a CHF size of 125 µm. Then, the strength dropped with the increased CHF sizes of 200 and 300 µm. The smaller fibre size composites of 125 µm demonstrated superior tensile performance compared to the larger fibre composites, with fibres widely scattered throughout the matrix. The increased fibre-matrix surface contact led to reduced fibre aggregation. It indicates that solid interfacial adhesion was obtained between the components of hybrid composites, which increased stress-transfer efficiency in the TPCS/CHF matrix. Similarly, identical findings were noted by Diyana et al. (2021a). Using larger 300 µm fibre contents considerably reduced the composites' strength qualities. In spite of this fact, this contrasts with Mohamed et al. (2018) findings that extending fibre length enhances tensile strength. Consequently, it was determined that an increase in fibre size decreased the absorption of specific energy of hot-pressed fibre composite materials with a 300 µm fibre size. This outcome can be attributed to the fact that despite using a small fibre size, it still offers a larger surface area for interaction with TPS. Consequently, the greater aspect ratio of the fibre promotes stress transmission to the matrix (Santos et al., 2018).

In this study, the measured mechanical strength fracture exhibited ductile features. Figure 5 presents the results of the tensile modulus of CHF composites with different fibre sizes of 0%, 125, 200, and 300 µm. Including CHF fibre increased the tensile modulus of 0% fibre from 5.8 to 880.8 MPa, the optimum tensile modulus obtained at 125µm. Thus, the smaller the fibre size of the CHF, the greater the tensile modulus, and vice versa. When the chopped fibre length or diameter was smaller, weaker tensile strength and stiffness were determined. This statement is aligned with previous work by Jacob et al. (2005). Specifically, fibre packing is much improved for smaller fibre sizes, reducing modulus for larger ones.

With an increase in fibre sizing of 200 and 300 µm, the tensile modulus decreased to 395.7 and 172.3 MPa, respectively. The reason is that increasing fibre size decreases matrix content while decreasing ductility results in a stiffer composite. Moreover, at this fibre size, there was less fibre-matrix interaction. It is due to the decreased intermolecular contact between starch molecules, which results in a larger free volume and greater chain mobility (Aji et al., 2011).

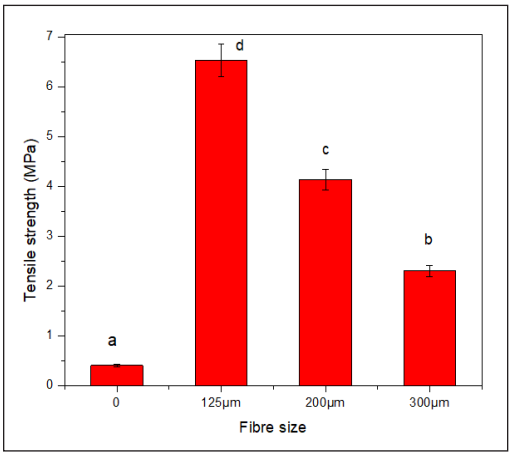

Figure 4. Tensile strength of coconut fibre composites with different fibre sizes (MPa)

Figure 6 shows the tensile strain of fibre sizes 0%, 125, 200, and 300 µm at break. It was shown that with the addition of CHF, the tensile strain at failure dropped simultaneously from 35.7 to 1.5%, decreasing the composite's stiffness. It was ascribed to the poor internal contact of larger

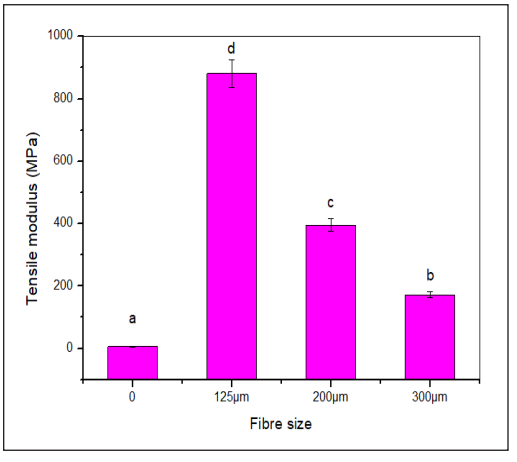

Figure 5. Tensile modulus of coconut fibre composition with different fibre sizes (MPa)

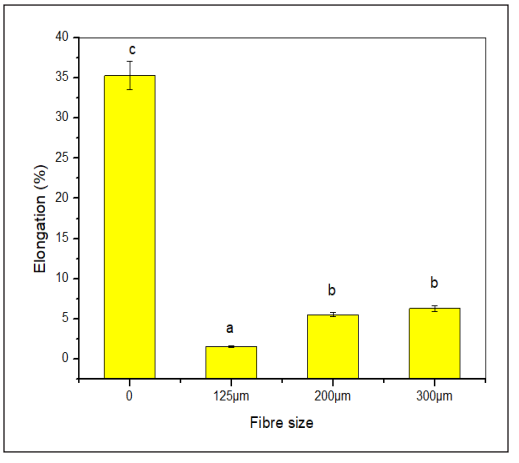

Figure 6. The tensile strain of coconut fibre composition with different fibre sizes (MPa)

fibres and the incapacity of larger fibres to bear the matrix-transferred strain (Prakash et al., 2021). According to Prasad et al. (2019), integrating natural fibre's fragility impeded the polymer chains' mobility in the matrix. The composites became stiffer when the elasticity ratio of matrix phases was substituted by increased fibre size content. For 125 µm fibre size, the composites demonstrated elongation at 1.5% fibre. According to Wollerdorfe and Bader (1998) and Yokesahachart et al. (2021), the size of the fibres affects the stress concentration at the ends of the fibres, which results in less elongation at fibre breaks for bigger fibres since the force cannot sustain local failure. Meanwhile, the tensile strain increased with the addition of larger fibre sizes of 200 and 300 µm to 5.5% and 6.3%, respectively. Decreasing the size diameter of the CHF led to greater stress on the composites.

Flexural Testing

Figure 7 shows the flexural strength of composite with CHF sizes 0%, 125, 200, and 300 µm, respectively. With fibre addition, the flexural strength rose to the highest strength of 13.8 MPa at 125 µm from 2.4 MPa, indicating the fibre-matrix interfacial adhesion facilitating increased stress transmission. It suggested the degree of cross-linking between molecular chains in the blends. The cross-linking of palm wax had favourably influenced the flexural strength and elasticity modulus, as indicated by a prior study describing the enhancement in flexural strength of corn starch mixed with kaolin and beeswax (Polat et al., 2013). The improvement in the flexural characteristics of the TPCS/CHF composites could be attributable to identical causes in the tensile findings.

Afterwards, the strength slightly decreased to 9.8 MPa at 200 µm before increasing again to 12.0 MPa at 300 µm. Owing to the low interfacial adhesion between reinforcement and matrix, an increase in fibre sizes of 200 µm diminished both strength and modulus attributes. It could be because the TPCS's palm wax failed to act as a reinforcing agent due to agglomerates and an uneven distribution. Additionally, because of the excess palm wax content associated with forming large agglomerates and phase separation, poor particle distribution resulted in poor mechanical distribution, similar to the tensile results reported by Ilyas et al. (2018).

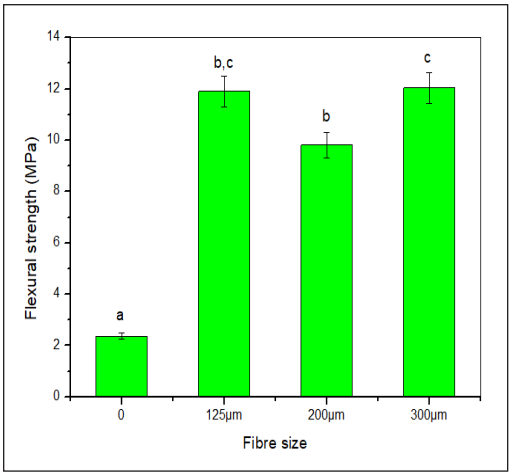

Figure 7. Flexural strength of TPCS/CHF composites with different fibre sizes (MPa)

As presented in Figure 8, the maximum flexural modulus of the CHF-reinforced TPCS composite was raised from 16.5 MPa at 0% fibre to 118.8 MPa at 125 µm. Then, the

particle reinforcement strength decreased to 320.8 MPa for 200 µm before rising to 532.2 MPa for 300 µm. This decrease was caused by the presence of voids or the formation of cracks at the composite's interface, the inability of the particle to endure the stresses transferred from the matrix, and the ineffective particle-matrix interfacial bonding, which resulted in a weak structure. However, the excessive fibre sizes of 300 µm elevated fibre elasticity and matrix to transmit stress. It enhanced the flexural modulus of the composites due to the composites' higher stiffness, including CHF in the matrix, and reduced polymeric chain mobility.

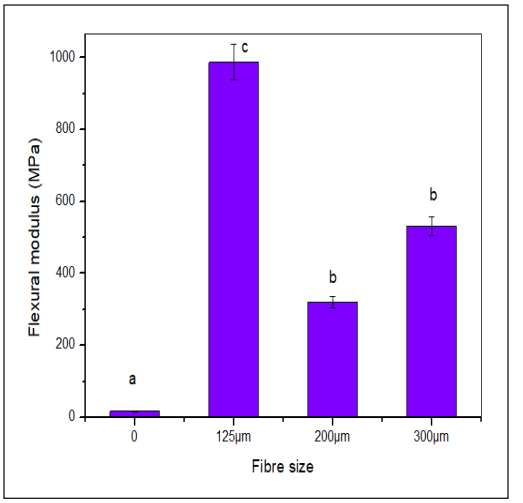

Figure 8. Flexural modulus of TPCS/CHF composites with different fibre sizes (MPa)

Seth et al. (2018), who researched the influence of particle size and loading on polypropylene-reinforced doum palm shell particle composites, obtained similar results. Literature documented a composite's properties improvement with decreasing particle size because smaller particles have greater compaction and reduced porosity, which results in effective stress transfer between the matrix and the particles. The tensile and flexural test results were subjected to statistical analysis using one-way ANOVA, and the results are presented in Table 2. The test's p-value was less than 0.05, showing statistically significant differences in the mixtures' average thermoplastic blend values for tensile and flexural strengths.

Table 2
Analysis of variance (ANOVA) summary of tensile and flexural properties

Variables	df	Tensile strength	Tensile strain	Tensile modulus	Flexural strength	Flexural modulus
Mixture	4	0.00*	0.00*	0.00*	0.00*	0.00*

Thermal Properties

The thermal properties and stability of TPCS-reinforced CHF composites were assessed by plotting the TGA curves as the percentage of sample weight loss versus temperature (°C), as shown in Figure 9(a). As the temperature rose, the weight percentage decreased, indicating continual mass changes due to thermal treatment. The three-step deterioration process was distinguished for all composites and their constituent materials. At about 100 and 160°C, the weight losses were due to the evaporation of water and glycerol, respectively. Relative to Sanyang et al. (2015), the earliest stage of degradation that occurs

at temperatures below 100°C is in relation to the dehydration of loosely bound water and low molecular weight compounds.

The mixtures of TPCS and CHF composites altered the thermal decomposition of the composites in numerous ways. At 250°C, the native TPCS began to degrade, representing the temperature at which samples started to deviate from the baseline and weight loss was ready to commence. The highest weight loss rate was reported at 318°C, according to the curve in Figure 9(a). Following Abral et al. (2019), when the temperature hits 180 to 360°C, the second phase of weight loss occurs due to starch's volatile breakdown. It was discovered that adding CHF to CFC1, CFC2, and CFC3 composites increased their onset and maximum degradation temperatures, as shown in Table 3. The composites' heat conductivity decrement with coir fibre addition was due to TPCS having more lignocellulose than CHF, which increased thermal stability. Besides, the CHF is less hydrophilic than the matrix, allowing quicker moisture evaporation when heated (Jumaidin et al., 2020). Parallel outcomes were discovered by Sarifuddin et al. (2012) and M. Hasan et al. (2020). At 350°C, CHF entered its final phase of disintegration.

Based on the graph in Figure 9(a), composites with 125 µm fibre size (CFC1) needed a lower temperature compared to larger-size CFC2 and CFC3 before losing weight percentage due to water loss. It is also reported that the maximum temperature value observed was 291°C, lower than the 336°C provided in the study by Diyana et al. (2021b). The discrepancies may be attributable to the varied parameter conditions during testing. According to Prachayawarakorn et al. (2012), using a variable fibre size may raise the temperature at which TPCS begins to degrade.

Furthermore, the thermal degradation of TPCS/CHF composites that led to the weight loss was found between 280 and 352°C. Figure 9(a) shows that the water weight loss percentage dropped significantly by including larger fibre. Hence, the larger the size of the fibre, the higher the temperature needed to lose water percentage. Adding larger CHF caused the CFC3 degradation temperature to drop when 300 µm fibres were used. This study suggested that larger-size CHF may enhance the thermal stability of composites through hydrogen bond interactions between the fibre and matrix, which corresponded to Javaid et al. (2020). At this point, the increase in fibre-size content from 125 to 300 µm has suggested that CHF is primarily responsible for the increase in degradation rate.

The thermal degradation and stability of TPCS/CHF composites were assessed by plotting the DTG curves as the derivative weight loss (mg $°C^{-1}$ versus temperature (°C), as shown in Figure 9(b). The curves denote that the most significant breakdown temperature of the native TPCS was around 318°C. It could be explained by the

Table 3
TGA findings of TPCS/CHF composites on the onset temperature, T_{on} (°C)

Samples	Ton (°C)
TPCS (reference)	318
CFC 1 (125 µm)	304
CFC 2 (200 µm)	305
CFC 3 (300 µm)	305

interactions between the polar side groups in the starch (e.g., hydroxyl carbonyl) and wax fraction in native TPCS, which has a high initial breakdown temperature (Halal et al., 2016).

With fibre inclusion in Figure 9(b), the highest DTG peak was observed between the temperature range of 250 and 350°C. However, when the fibre was added, the DTG peaks decreased, and only very slight variations were found (Sahari et al., 2013). A rapid weight loss took place due to the decomposition of fibre, starch, and glycerol, creating volatile matters, e.g., carbon monoxide (CO) and carbon dioxide (CO_2) (Hassan et al., 2019). Monteiro et al. (2012) reported that the initial phase of the DTG peak is related to moisture release. The breakdown of fibre began in the second phase, as represented by the primary DTG peak. Cellulose degradation is indicated at the peak, whereas hemicellulose and lignin decompositions occur at the shoulder and tail peaks. The residue at the end of the process might be ascribed to the solid char from the degradation events. The DTG curve is crucial for better insight into the composite material's thermal decomposition behaviour.

This observation is in accordance with research done by Tajvidi and Takemura (2010), who investigated the heat deterioration of natural fibre reinforced with polypropylene (PP), woof flour composites, and kenaf fibre. The wood flour composites and kenaf fibre had high breakdown rates in three phases. The initial step began at the temperature range of 250 and 300°C and was linked to hemicellulose and PP breakdown. The second stage was initiated at 300°C and continued up to 400°C, describing cellulose degradation. The ultimate decomposition was detected at about 450°C.

Razali et al. (2015) previously studied char as the residue after the pyrolysis of all volatile matter in a substance. The char residue concentration of TPCS/CHF composites rose with the addition of CHF, with CFC3 containing the most char residue at 49.33% (7.94 mg). Based on the TGA study, it is summarised that the CHF inclusion enhanced the charring and thermal stability of the TPCS/CHF composite.

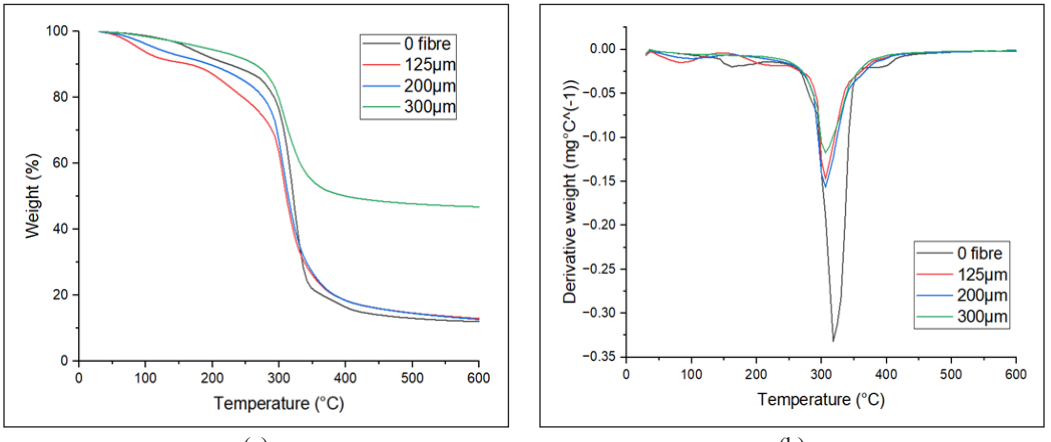

(a) (b)

Figure 9. (a) TGA and (b) DTG curves on TPCS/CHF composites

FTIR Analysis

The Fourier transform infrared (FT-IR) analysis revealed the high content of chemical components in coir materials. The FT-IR findings for TPCS/CHF composites from 0 to 300 µm of fibre size contents are shown in Figure 10. All spectra of TPCS composites displayed comparable patterns, demonstrating that the TPCS was unaffected by the size of the coconut husk fibre in all composite samples. A broad wavelength range between 3000 and 3700 cm^{-1} matched the hydroxyl group (-OH) stretching vibrations ascribed with the complicated vibrational stretching of free-, inter-, and intra-molecularly bonded hydroxyl groups (AL-Hassan & Norziah, 2017; Hafila et al., 2022). This discovery demonstrated new matrix-fibre hydrogen bond formations that relate to fibre addition. Notably, the slightly smaller C-O stretching peak in TPCS compared to TPCS/CHF at 1338 cm^{-1} is probably due to the reorganisation of hydrogen bonds between starch and fibre (Sarifuddin et al., 2012). Changes in the IR spectrum revealed a specific interaction and compatibility between polymer chains.

In Figure 10, the band at around 2916 cm^{-1} was attributed to C–H stretching from CH_2 or CH_3 or conjugated bending vibrations, which were present in all composite samples. Like Barkoula et al. (2008), this band coincided with natural fibre's cellulose and hemicellulose constituents. The existence of hydroxyl groups led to the starch being very sensitive to water molecules (Ilyas et al., 2018; Sahari et al., 2013). It was also linked to the hydroxyl groups stretching due to the molecules' hydrogen bonds. Pursuant to Dang and Yoksan (2021), the peak around 2916 cm^{-1} corresponds to C–H stretching (-CH_2) of the anhydroglucose ring (Zullo & Iannace, 2009), while the peak at around 3277 cm^{-1} is associated to the firmly bound water exist in the starch structure (Zhang & Han, 2006) owing to its hygroscopic nature.

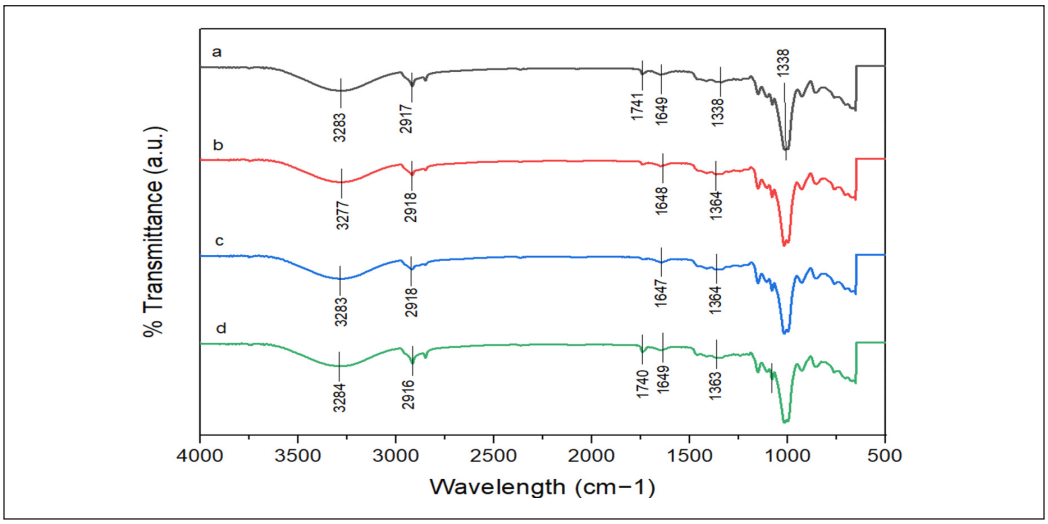

Figure 10. FTIR spectrum of TPCS with (a) 0%, (b) 125 µm, (c) 200 µm, and (d) 300 µm fibre

According to Lomelí-Ramírez et al. (2014), the band at around 1725 cm^{-1} may correspond to stretching vibrations of carbonyl groups (C=O). However, when the larger fibre was used, the O–H bond peak moved to a lower wavenumber before arising to a higher frequency, indicating an increase in the average strength of hydrogen bonds. Sample with no fibre (Figure 10 a) reached a maximum peak of 3283 cm^{-1}, whereas specimens with the largest fibre size, 300 µm (Figure 10 (d), reached a maximum peak of 3284 cm^{-1}. In a prior Prachayawarakorn et al. (2011) study, TPCS/kapok and TPCS/jute fibres exhibited a comparable O–H pattern.

It is related to starch containing hydroxyl (OH) functional groups in their basic structure. The tensile result was substantiated at the OH peak regions at 3277 and 3284 cm^{-1}. Meanwhile, the decrease in elongation following fibre addition might be due to starch-fibre matrix bonding, which precluded considerable material elongation. As a result, the composite matrix lost some of its ductility. It may be assumed that the resulting bio-composite became tougher, more brittle, and less flexible as the diameter was increased.

XRD Analysis

The presence of cellulose and amorphous fractions in the fibre was verified by XRD analysis. Figure 11 illustrates the diffraction patterns of the three native starches employed. Starch granules display, in general, two primary kinds of X-ray diffraction patterns called A and B crystal structures. These two allomorphs assume that the crystalline domains are generated for the short terminal segments of amylopectin molecules with identical double-helical shapes but distinct packing arrangements and differing intercrystalline water content. The A-type structure is usually present in cereal starches, whereas the B-type structure is prevalent in starches from tubers or rich amylose carbohydrates (Montero et al., 2017).

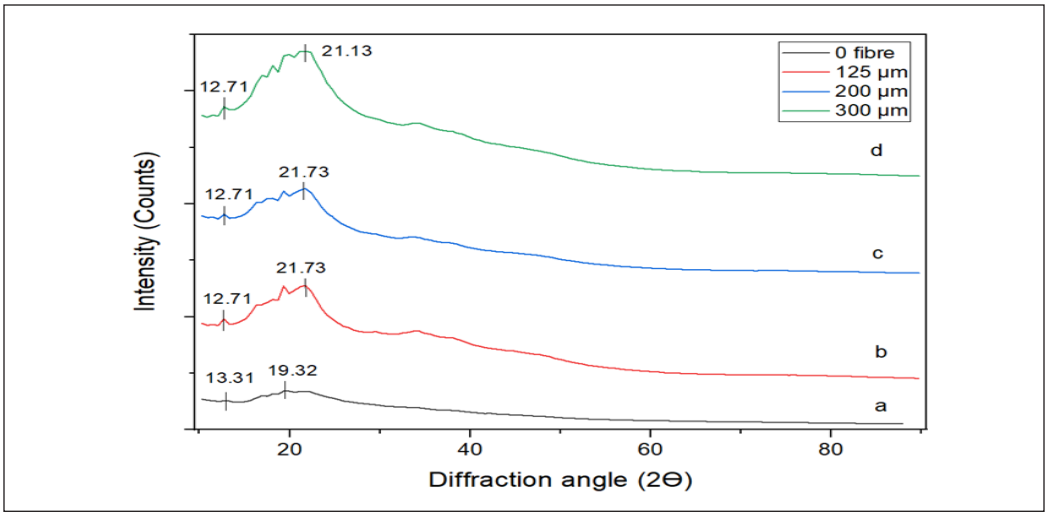

Figure 11. XRD analysis on TPCS/CHF with (a) 0%, (b) 125 µm, (c) 200 µm, and (d) 300 µm fibre

The study by Moura et al. (2019) compared the composites reinforced with larger-sized and small-sized fibres. The smaller fibre-reinforced composites exhibited a higher crystallinity and melting temperature. According to the XRD analysis, the fibre diameter and crystallinity dropped and increased during the bleaching or heating of the raw coir fibres. Abraham et al. (2013) stated that it would cause the fibre to inflate, leading to an increase in the fibre's reactive surface area. Consequently, it was verified by Dong et al. (2014) that coir fibres performed an efficient nucleating function to expedite the polylactic acid (PLA) crystallisation process, thus increasing the crystal growth rate.

XRD patterns of all samples are shown in Figure 11. The spectrum of TPCS revealed only a semi-crystalline substance with small crystalline peaks at 2-theta values between 13.31 and 19.32°, which corresponded to the processing-induced crystal of amylose-glycerol complexes of the Vh-type (Kaewtatip & Tanrattanakul, 2012; Yokesahachart et al., 2021). The TPCS/CHF matrices displayed prominent diffraction peaks at $2\theta = 21.73°$ (300 μm), suggesting a typical A-type pattern (Kamaruddin et al., 2022). It may be related to the unstable single helix structure complexation of amylose and plasticiser containing a low quantity of water. Relative to Agyei-Tuffour et al. (2021), the higher the composite's crystallinity, the harder and more brittle it becomes.

The diffraction peaks of TPCS rose after the inclusion of CHF, primarily exhibiting a V-type crystal as the CHF sizes continued to rise (Liu et al., 2022). Thus, the percentage crystallinity of TPCS-based composites increased as CHF fibre size increased. After the gelatinisation process, the crystalline structure of TPCS was created by the fast retrogradation or recrystallisation of starch molecules. However, with further mixing with a larger fibre size of 300 μm, the diffractograms peak at 2Θ dropped to 39.85% due to the aggregation of CHFs, resulting in a less heterogeneous nucleation action and slowed starch molecule movements (Yokesahachart et al., 2021).

Besides, the analysis revealed that the inclusion of the CHF particle sizes of 125 and 200 μm increased most of the crystallinity of the TPCS/CHF composite. The crystallinity of the sample was enhanced when the TPCS was reinforced with fibres of a larger diameter. It was likely attributable to the larger CHF size exhibiting a smaller surface area ratio. Hence, it was predicted that raising the size diameter of CHF in the samples would enhance their relative crystallinity. Similar findings were noted by Liu et al. (2022). According to Dang and Yoksan (2021), the crystallinity also increased with increasing temperature and pressure during extrusion owing to the amylose release resulting from the more significant disruption of the starch granule structure. Moreover, the total crystallinity of the TPCS/CHF composites rose with rising CHF sizes, perhaps owing to the high CHF crystallinity. A parallel conclusion was reported for thermoplastic cassava starch/cassava bagasse composites reinforced with sugar palm fibre by Edhirej et al. (2017) and TPCS/PLA blend reinforced with coir fibres by Chotiprayon et al. (2020).

It could be described by the heterogeneous nucleation impact of CHF on starch recrystallisation. Nevertheless, the composites containing CHF revealed a lower peak intensity at 2Θ of 12.71° due to the aggregation of CHFs generating a declined heterogeneous nucleation effect and the slowed movements of starch molecules. The computed crystalline index content in the TPCS matrix was 31.11% (Table 4).

Table 4
Index crystallinity of TPCS/CHF composites

Samples	Crystallinity Index (%)
TPCS	31.11
CFC 125	41.51
CFC 200	41.51
CFC 300	39.85

SEM Analysis

The surface morphology of the tensile fractured surface was examined using scanning electron microscopy (SEM). The porosity of samples was determined by the voids present, which are the result of fibre packing. The coconut husk fibres (CHF) and the matrix demonstrated good compatibility and adhesion. According to Prachayawarakorn et al. (2011), the size, chemical composition, and shape of the fibre directly impact the interfacial adhesion between the fibre and polymer matrix, homogenisation in the distribution with the polymer matrix, and subsequently, the affinity between the two materials. These characteristics are essential for the composite's mechanical performance.

Figure 12 arrays the SEM images of the fractured surface microstructures with various fibre sizes: 0%, 125, 200, and 300 μm. Figure 12(a) demonstrates the TPCS matrix exhibiting a continuous surface without voids, creasers, or distinct starch portions. No starch aggregates or inflated granules were visible on this surface; hence, the plasticiser was thought to have broken the inter- and intra-molecular hydrogen bonding in native cassava starch, appropriately completing the plasticisation process. Then, the CHF was effectively encoded into the TPCS matrix. It is feasible to see fibres emerging from the composite's fracture surface in Figures 12 (b, c, and d).

The fracture surfaces' microstructure demonstrated ductile tearing with some fibre breakings. It is attributable to poor fibre-matrix interface adhesion. These observations aligned with the tensile results reported by Diyana et al. (2021a). Meanwhile, in Figure 12(d), it was noticed that the samples' surfaces displayed decreased homogeneity, yielding a non-uniform and stiff structure with an uneven surface and the presence of voids. It can be linked to the starch-CHF interaction that was comparatively low due to the inclusion of larger-size fibres and the lack of appropriate hydrophilic starch mixed with a hydrophobic fibre matrix (Hafila et al., 2022). Due to discontinuity in the matrix and agglomeration, it started at a larger fibre content.

Figure 13 depicts the focused SEM images of TPCS/CHF composites. The close-up detail of native cassava starch granules can be seen with 150 μm magnification, as

presented in Figure 13(a). Cassava starch granules are spherical with a truncated end and a well-defined hilum. The granule sizes are between 5 and 35 μm. The existence of starch granules indicated the efficiency of shear- and thermo-processing at gelatinising the starch granules. However, the starch granules were not noticeably visible, indicating the starch was well plasticised in Figures 13 (b, c, d, and e).

Fragmentation of the fibres was seen in all composites as a consequence of tensile fracture caused by the reinforcing effect of the matrix's stress transmission to the fibres (Jumaidin et al., 2021). Meanwhile, including CHF in TPCS composites produced a rough structure with CHF on its surface. It can be shown in Figure 13(e) that CHF and TPCS are highly compatible, as evidenced by the matrix's adequate fibre wetting. A previous study reported that the length of the fibres impacts the stress concentration at the fibre ends, resulting in less elongation at fibre breaks for longer fibres since the system cannot withstand local failure (Delli et al., 2021). In addition, more fibre-size ends are present in composites, leading to failure at lower stresses. It is also in perfect accord with the previously disclosed Young's modulus and yield strength values. Parallel findings were discovered by Khalaf et al. (2021) and Salasinska et al. (2015). The morphological examination indicated excellent interfacial adhesion, demonstrating the matrix's inherent affinity with the reinforcement without using chemicals that harm the environment.

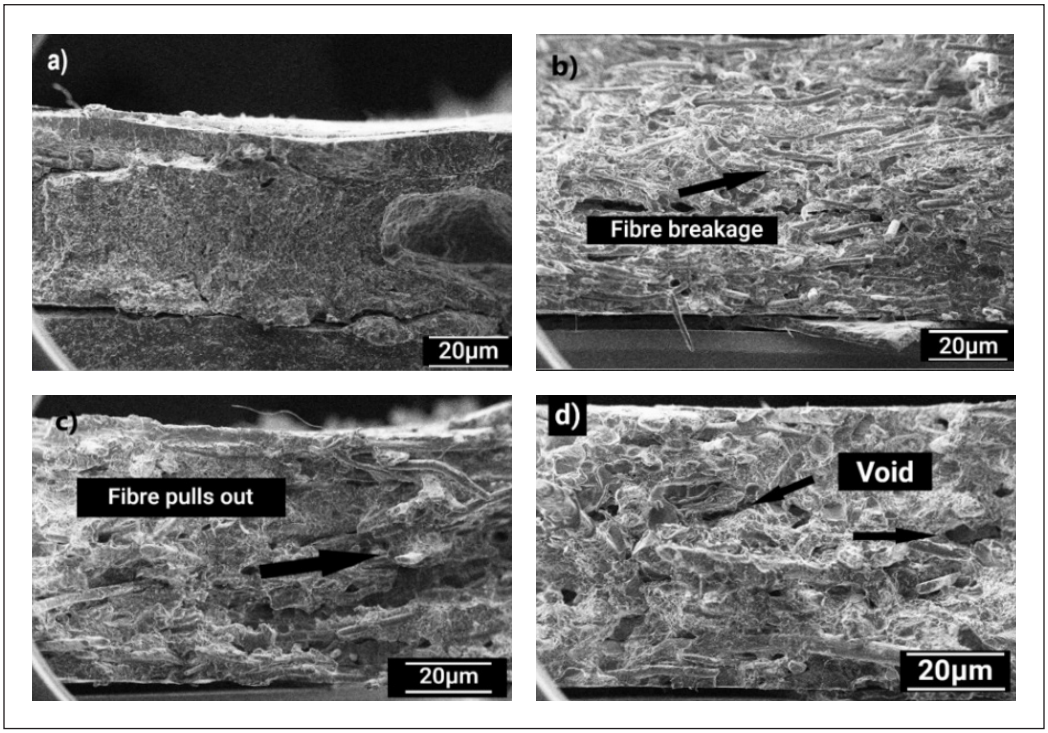

Figure 12. SEM images of fracture surfaces of TPCS/CHF with different fibre sizes: (a) 0 fibre, (b) 125 μm, (c) 200 μm, and (d) 300 μm

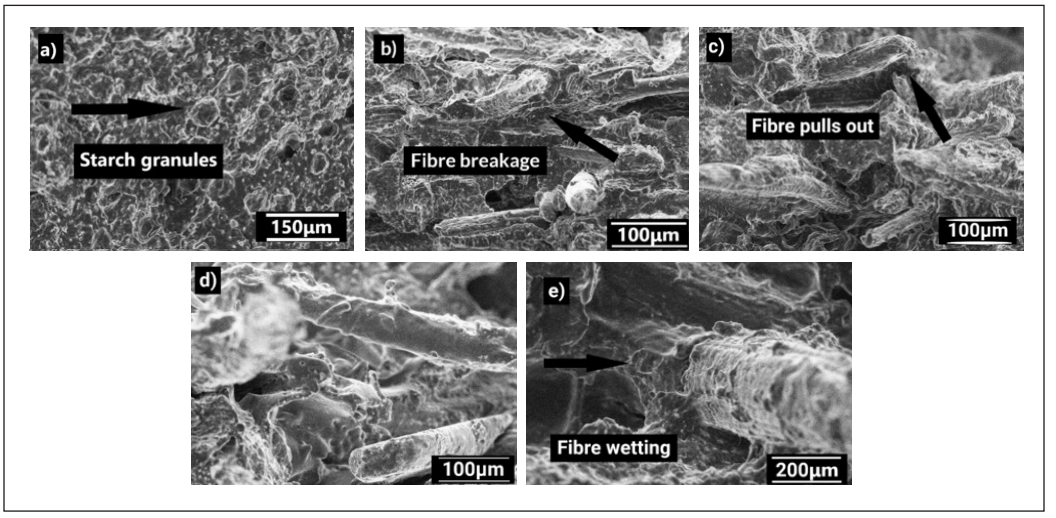

Figure 13. SEM images of shattered surface microstructures with various fibre sizes

CONCLUSION

The biodegradable TPCS reinforced with coconut husk fibre composite has been successfully prepared at 125, 200, and 300 µm fibre using dry mixing and hot-pressed methods. The addition of fibre increased tensile and flexural strength as well as modulus. Composites with a fibre size of 125 µm showed the highest tensile of 6.5 MPa and flexural strength of 13.8 MPa. In general, mixing the cassava starch with the fibre improved the thermal stability of the composites, while smaller fibre sizes led to better mechanical properties. The FTIR and SEM results also depict that cassava starch and coconut husk fibre were compatible and could form a homogenous structure. Overall, TPCS-reinforced coconut husk fibre has shown promise as an alternative to non-environmentally friendly polymers.

ACKNOWLEDGEMENTS

The authors thank Universiti Teknikal Malaysia Melaka and the Ministry of Higher Education Malaysia for the financial support through research grant FRGS/1/2023/STG05/UTEM/02/2.

REFERENCES

Abdullah, A., Jamaludin, S. B., Noor, M. M., & Hussin, K. (2011). Composite cement reinforced coconut fibre: Physical and mechanical properties and fracture behaviour. *Australian Journal of Basic and Applied Sciences*, *5*(7), 1228–1240.

Abraham, E., Deepa, B., Pothen, L. A., Cintil, J., Thomas, S., John, M. J., Anandjiwala, R., & Narine, S. S. (2013). Environmental friendly method for the extraction of coir fibre and isolation of nanofibre. *Carbohydrate Polymers*, *92*(2), 1477–1483. https://doi.org/10.1016/j.carbpol.2012.10.056

Abral, H., Basri, A., Muhammad, F., Fernando, Y., Hafizulhaq, F., Mahardika, M., Sugiarti, E., Sapuan, S. M., Ilyas, R. A., & Stephane, I. (2019). A simple method for improving the properties of the sago starch films prepared by using ultrasonication treatment. *Food Hydrocolloids*, *93*, 276–283. https://doi.org/10.1016/j.foodhyd.2019.02.012

Agyei-Tuffour, B., Asante, J. T., Nyankson, E., Dodoo-Arhin, D., Oteng-Peprah, M., Azeko, S. T., Azeko, A. S., Oyewole, O. K., & Yaya, A. (2021). Comparative analyses of rice husk cellulose fibre and kaolin particulate reinforced thermoplastic cassava starch biocomposites using the solution casting technique. *Polymer Composites*, *42*(7), 3216–3230. https://doi.org/10.1002/pc.26052

Aji, I. S., Zainudin, E. S., Khalina, A., Sapuan, S. M., & Khairul, M. D. (2011). Studying the effect of fibre size and fibre loading on the mechanical properties of hybridized kenaf/PALF-reinforced HDPE composite. *Journal of Reinforced Plastics and Composites*, *30*(6), 546–553. https://doi.org/10.1177/0731684411399141

AL-Hassan, A. A., & Norziah, M. H. (2017). Effect of transglutaminase induced crosslinking on the properties of starch/gelatin films. *Food Packaging and Shelf Life*, *13*, 15–19. https://doi.org/10.1016/j.fpsl.2017.04.006

ASTM [American Society for Testing and Materials]. (2022). *ASTM D638 Standard test method for tensile properties of plastics.* ASTM International.

ASTM [American Society for Testing and Materials]. (2017). *ASTM D790 Standard test methods for flexural properties of unreinforced and reinforced plastics and electrical insulating materials*. ASTM International.

Barkoula, N. M., Alcock, B., Cabrera, N. O., & Peijs, T. (2008). Flame-retardancy properties of intumescent ammonium poly(Phosphate) and mineral filler magnesium hydroxide in combination with graphene. *Polymers and Polymer Composites*, *16*(2), 101–113. https://doi.org/10.1002/pc

Campos, A., Sena Neto, A. R., Rodrigues, V. B., Luchesi, B. R., Mattoso, L. H. C., & Marconcini, J. M. (2018). Effect of raw and chemically treated oil palm mesocarp fibres on thermoplastic cassava starch properties. *Industrial Crops and Products*, *124*, 149–154. https://doi.org/10.1016/j.indcrop.2018.07.075

Ceseracciu, L., Heredia-Guerrero, J. A., Dante, S., Athanassiou, A., & Bayer, I. S. (2015). Robust and biodegradable elastomers based on corn starch and polydimethylsiloxane (PDMS). *ACS Applied Materials and Interfaces*, *7*(6), 3742–3753. https://doi.org/10.1021/am508515z

Chotiprayon, P., Chaisawad, B., & Yoksan, R. (2020). Thermoplastic cassava starch/poly(lactic acid) blend reinforced with coir fibres. *International Journal of Biological Macromolecules*, *156*, 960–968. https://doi.org/10.1016/j.ijbiomac.2020.04.121

Dang, K. M., & Yoksan, R. (2021). Thermoplastic starch blown films with improved mechanical and barrier properties. *International Journal of Biological Macromolecules*, *188*, 290–299. https://doi.org/10.1016/j.ijbiomac.2021.08.027

Delli, E., Giliopoulos, D., Bikiaris, D. N., & Chrissafis, K. (2021). Fibre length and loading impact on the properties of glass fibre reinforced polypropylene random composites. *Composite Structures, 263*, Article 113678. https://doi.org/10.1016/j.compstruct.2021.113678

Diyana, Z. N., Jumaidin, R., Selamat, M. Z., Alamjuri, R. H., & Yusof, F. A. M. (2021a). Extraction and characterization of natural cellulosic fibre from pandanus amaryllifolius leaves. *Polymers*, *13*(23), Article 4171. https://doi.org/10.3390/polym13234171

Diyana, Z. N., Jumaidin, R., Selamat, M. Z., & Suan, M. S. M. (2021b). Thermoplastic starch/beeswax blend: Characterization on thermal mechanical and moisture absorption properties. *International Journal of Biological Macromolecules*, *190*, 224–232. https://doi.org/10.1016/j.ijbiomac.2021.08.201

Dong, Y., Ghataura, A., Takagi, H., Haroosh, H. J., Nakagaito, A. N., & Lau, K. T. (2014). Polylactic acid (PLA) biocomposites reinforced with coir fibres: Evaluation of mechanical performance and multifunctional properties. *Composites Part A: Applied Science and Manufacturing*, *63*, 76–84. https://doi.org/10.1016/j.compositesa.2014.04.003

Edhirej, A., Sapuan, S. M., Jawaid, M., & Zahari, N. I. (2017). Preparation and characterization of cassava bagasse reinforced thermoplastic cassava starch. *Fibers and Polymers*, *18*(1), 162–171. https://doi.org/10.1007/s12221-017-6251-7

Estrada-Monje, A., Alonso-Romero, S., Zitzumbo-Guzmán, R., Estrada-Moreno, I. A., & Zaragoza-Contreras, E. A. (2021). Thermoplastic starch-based blends with improved thermal and thermomechanical properties. *Polymers*, *13*(23), Article 4263. https://doi.org/10.3390/polym13234263

Hafila, K. Z., Jumaidin, R., Ilyas, R. A., Selamat, M. Z., & Yusof, F. A. M. (2022). Effect of palm wax on the mechanical, thermal, and moisture absorption properties of thermoplastic cassava starch composites. *International Journal of Biological Macromolecules*, *194*, 851–860. https://doi.org/10.1016/j.ijbiomac.2021.11.139

Halal, S. L. M. E., Zavareze, E. D. R., Rocha, M. D., Pinto, V. Z., Nunes, M. R., Luvielmo, M. D. M., & Prentice, C. (2016). Films based on protein isolated from croaker (*Micropogonias furnieri*) and palm oil. *Journal of the Science of Food and Agriculture*, *96*(7), 2478–2485. https://doi.org/10.1002/jsfa.7368

Hasan, M., Gopakumar, D. A., Olaiya, N. G., Zarlaida, F., Alfian, A., Aprinasari, C., Alfatah, T., Rizal, S., & Khalil, H. P. S. A. (2020). Evaluation of the thermomechanical properties and biodegradation of brown rice starch-based chitosan biodegradable composite films. *International Journal of Biological Macromolecules*, *156*, 896–905. https://doi.org/10.1016/j.ijbiomac.2020.04.039

Hassan, M. M., Le Guen, M. J., Tucker, N., & Parker, K. (2019). Thermo-mechanical, morphological and water absorption properties of thermoplastic starch/cellulose composite foams reinforced with PLA. *Cellulose*, *26*(7), 4463–4478. https://doi.org/10.1007/s10570-019-02393-1

Hazrol, M. D., Sapuan, S. M., Zainudin, E. S., Zuhri, M. Y. M., & Wahab, N. I. A. (2021). Corn starch (*Zea mays*) biopolymer plastic reaction in combination with sorbitol and glycerol. *Polymers*, *13*(2), Article 242. https://doi.org/10.3390/polym13020242

Ilyas, R. A., & Sapuan, S. M. (2020a). Biopolymers and biocomposites: Chemistry and technology. *Current Analytical Chemistry*, *16*(5), 500–503. https://doi.org/10.2174/1573411016052006030953 11

Ilyas, R. A., & Sapuan, S. M. (2020b). The preparation methods and processing of natural fibre bio-polymer composites. *Current Organic Synthesis*, *16*(8), 1068–1070. https://doi.org/10.2174/1570179416082001 20105616

Ilyas, R. A., Sapuan, S. M., Ishak, M. R., & Zainudin, E. S. (2018). Development and characterization of sugar palm nanocrystalline cellulose reinforced sugar palm starch bionanocomposites. *Carbohydrate Polymers*, *202*, 186–202. https://doi.org/10.1016/j.carbpol.2018.09.002

Ilyas, R. A., Zuhri, M. Y. M., Norrrahim, M. N. F., Misenan, M. S. M., Jenol, M. A., Samsudin, S. A., Nurazzi, N. M., Asyraf, M. R. M., Supian, A. B. M., Bangar, S. P., Nadlene, R., Sharma, S., & Omran, A. A. B. (2022). Natural fiber-reinforced polycaprolactone green and hybrid biocomposites for various advanced applications. *Polymers, 14*(1), Article 182. https://doi.org/10.3390/polym14010182

Jacob, G. C., Starbuck, J. M., Fellers, J. F., & Simunovic, S. (2005). Effect of fibre volume fraction, fibre length and fibre tow size on the energy absorption of chopped carbon fibre-polymer composites. *Polymer Composites*, *26*(3), 293–305. https://doi.org/10.1002/pc.20100

Javaid, M. A., Zia, K. M., Zafar, K., Khosa, M. K., Akram, N., Ajmal, M., Imran, M., & Iqbal, M. N. (2020). Synthesis and molecular characterisation of chitosan/starch blends based polyurethanes. *International Journal of Biological Macromolecules*, *146*, 243–252. https://doi.org/10.1016/j.ijbiomac.2019.12.234

Jumaidin, R., Diah, N. A., Ilyas, R. A., Alamjuri, R. H., & Yusof, F. A. M. (2021). Processing and characterisation of banana leaf fibre reinforced thermoplastic cassava starch composites. *Polymers, 13*, Article 1420. https://doi.org/10.3390/polym13091420

Jumaidin, R., Khiruddin, M. A. A., Asyul Sutan Saidi, Z., Salit, M. S., & Ilyas, R. A. (2020). Effect of cogon grass fibre on the thermal, mechanical and biodegradation properties of thermoplastic cassava starch biocomposite. *International Journal of Biological Macromolecules*, *146*, 746–755. https://doi.org/10.1016/j.ijbiomac.2019.11.011

Jusoh, M. S. M., Nordin, M. N., & Ahamad, W. M. A. W. (2021). Comparison study on fibre and cocopeat from young coconut husks and old coconut husks. *Advances in Agricultural and Food Research Journal*, *2*(2), Article a0000216. https://doi.org/10.36877/aafrj.a0000216

Kaewtatip, K., & Tanrattanakul, V. (2012). Structure and properties of pregelatinized cassava starch/kaolin composites. *Materials and Design*, *37*, 423–428. https://doi.org/10.1016/j.matdes.2011.12.039

Kamaruddin, Z. H., Jumaidin, R., Ilyas, R. A., Selamat, M. Z., Alamjuri, R. H., & Yusof, F. A. M. (2022). Biocomposite of cassava starch-cymbopogan citratus fibre: Mechanical, thermal and biodegradation properties. *Polymers*, *14*(3), Article 514. https://doi.org/10.3390/polym14030514

Khalaf, Y., El Hage, P., Dimitrova Mihajlova, J., Bergeret, A., Lacroix, P., & El Hage, R. (2021). Influence of agricultural fibres size on mechanical and insulating properties of innovative chitosan-based insulators. *Construction and Building Materials*, *287*, Article 123071. https://doi.org/10.1016/j.conbuildmat.2021.123071

Liu, Y., Liang, Z., Liao, L., & Xiong, J. (2022). Effect of sisal fibre on retrogradation and structural characteristics of thermoplastic cassava starch. *Polymers and Polymer Composites*, *30*, Article 09673911221080363. https://doi.org/10.1177/09673911221080363

Lomelí-Ramírez, M. G., Kestur, S. G., Manríquez-González, R., Iwakiri, S., De Muniz, G. B., & Flores-Sahagun, T. S. (2014). Bio-composites of cassava starch-green coconut fibre: Part II - Structure and properties. *Carbohydrate Polymers*, *102*(1), 576–583. https://doi.org/10.1016/j.carbpol.2013.11.020

Madhumitha, G., Fowsiya, J., Mohana Roopan, S., & Thakur, V. K. (2018). Recent advances in starch–clay nanocomposites. *International Journal of Polymer Analysis and Characterisation*, *23*(4), 331–345. https://doi.org/10.1080/1023666X.2018.1447260

Marichelvam, M. K., Jawaid, M., & Asim, M. (2019). Corn and rice starch-based bio-plastics as alternative packaging materials. *Fibres*, *7*(4), Article 32. https://doi.org/10.3390/fib7040032

Mina, J. H., Valadez, A., Franco, P. J. H., & Toledano, T. (2009). Influencia del tiempo de almacenamiento en las propiedades estructurales de un almidón termoplástico de yuca (TPS) [Influence of storage time on the structural properties of a cassava thermoplastic starch (TPS)]. *Ingeniería y Competitividad*, *11*(2), 1-26. https://doi.org/10.25100/iyc.v11i2.2461

Mohamed, W. Z. W., Baharum, A., Ahmad, I., Abdullah, I., & Zakaria, N. E. (2018). Effects of fibre size and fibre content on mechanical and physical properties of *Mengkuang* reinforced thermoplastic natural rubber composites. *BioResources*, *13*(2), 2945–2959. https://doi.org/10.15376/biores.13.2.2945-2959

Mo, X. Z., Zhong, Y. X., Liang, C. Q., & Yu, S. J. (2010). Studies on the properties of banana fibers-reinforced thermoplastic cassava starch composites: Preliminary results. *Advanced Materials Research*, *87–88*, 439–444. https://doi.org/10.4028/www.scientific.net/AMR.87-88.439

Monteiro, S. N., Calado, V., Rodriguez, R. J. S., & Margem, F. M. (2012). Thermogravimetric behaviour of natural fibres reinforced polymer composites-An overview. *Materials Science and Engineering A*, *557*, 17–28. https://doi.org/10.1016/j.msea.2012.05.109

Montero, B., Rico, M., Rodríguez-Llamazares, S., Barral, L., & Bouza, R. (2017). Effect of nanocellulose as a filler on biodegradable thermoplastic starch films from tuber, cereal and legume. *Carbohydrate Polymers*, *157*, 1094–1104. https://doi.org/10.1016/j.carbpol.2016.10.073

Moura, A. D. S., Demori, R., Leão, R. M., Frankenberg, C. L. C., & Santana, R. M. C. (2019). The influence of the coconut fiber treated as reinforcement in PHB (polyhydroxybutyrate) composites. *Materials Today Communications*, *18*, 191–198. https://doi.org/10.1016/j.mtcomm.2018.12.006

Polat, S., Uslu, M. K., Aygün, A., & Certel, M. (2013). The effects of the addition of corn husk fibre, kaolin and beeswax on cross-linked corn starch foam. *Journal of Food Engineering*, *116*(2), 267–276. https://doi.org/10.1016/j.jfoodeng.2012.12.017

Prachayawarakorn, J., Limsiriwong, N., Kongjindamunee, R., & Surakit, S. (2012). Effect of agar and cotton fiber on properties of thermoplastic waxy rice starch composites. *Journal of Polymers and the Environment*, *20*(1), 88–95. https://doi.org/10.1007/s10924-011-0371-8

Prachayawarakorn, J., Ruttanabus, P., & Boonsom, P. (2011). Effect of cotton fiber contents and lengths on properties of thermoplastic starch composites prepared from rice and waxy rice starches. *Journal of Polymers and the Environment*, *19*(1), 274–282. https://doi.org/10.1007/s10924-010-0273-1

Pradeep, M., Binoy, R. F., Yaswanth, S., Pullan, T. T., & Joseph, M. (2022). Investigations on chitin and coconut fibre reinforcements on mechanical and moisture absorption properties of corn starch bioplastics. *Materials Today: Proceedings, 58,* 65-70. https://doi.org/10.1016/j.matpr.2021.12.585

Prakash, K. B., Fageehi, Y. A., Saminathan, R., Manoj Kumar, P., Saravanakumar, S., Subbiah, R., Arulmurugan, B., & Rajkumar, S. (2021). Influence of fiber volume and fibre length on thermal and flexural properties of a hybrid natural polymer composite prepared with banana stem, pineapple leaf, and s-glass. *Advances in Materials Science and Engineering*, *2021*, Article 6329400. https://doi.org/10.1155/2021/6329400

Razali, N., Salit, M. S., Jawaid, M., Ishak, M. R., & Lazim, Y. (2015). A study on chemical composition, physical, tensile, morphological, and thermal properties of roselle fibre: Effect of fibre maturity. *BioResources*, *10*(1), 1803–1823. https://doi.org/10.15376/biores.10.1.1803-1824

Rivadeneira-Velasco, K. E., Utreras-Silva, C. A., Díaz-Barrios, A., Sommer-Márquez, A. E., Tafur, J. P., & Michell, R. M. (2021). Green nanocomposites based on thermoplastic starch: A review. *Polymers, 13*(19), Article 3227. https://doi.org/10.3390/polym13193227

Sahari, J., Sapuan, S. M., Zainudin, E. S., & Maleque, M. A. (2013). Mechanical and thermal properties of environmentally friendly composites derived from sugar palm tree. *Materials and Design*, *49*, 285–289. https://doi.org/10.1016/j.matdes.2013.01.048

Salasinska, K., & Ryszkowska, J. (2015). The effect of filler chemical constitution and morphological properties on the mechanical properties of natural fibre composites. *Composite Interfaces*, *22*(1), 39–50. https://doi.org/10.1080/15685543.2015.984521

Santos, B. H. D. Prado, K. D. S. D., Jacinto, A. A., & Spinace, M. A. D. S. (2018). Influence of sugarcane bagasse fiber size on biodegradable composites of thermoplastic starch. *Journal of Renewable Materials, 6*(2), 176–182. https://doi.org/10.7569/JRM.2018.634101

Sanyang, M. L., Sapuan, S. M., Jawaid, M., Ishak, M. R., & Sahari, J. (2015). Effect of plasticizer type and concentration on tensile, thermal and barrier properties of biodegradable films based on sugar palm (Arenga pinnata) starch. *Polymers*, *7*(6), 1106–1124. https://doi.org/10.3390/polym7061106

Sarifuddin, N., Ismail, H., & Ahmad, Z. (2012). Effect of fibre loading on properties of thermoplastic sago starch/kenaf core fibre biocomposites. *BioResources*, *7*(3), 4294–4306. https://doi.org/10.15376/biores.7.3.4294-4306

Seth, S. A., Aji, I. S., & Tokan, A. (2018). Effects of particle size and loading on tensile and flexural properties of polypropylene reinforced doum palm shell particles composites. *Technology, and Sciences (ASRJETS) American Scientific Research Journal for Engineering*, *44*(1), 231–239.

Syafiq, R., Sapuan, S. M., Zuhri, M. Y. M., Ilyas, R. A., Nazrin, A., Sherwani, S. F. K., & Khalina, A. (2020). Antimicrobial activities of starch-based biopolymers and biocomposites incorporated with plant essential oils: A review. *Polymers*, *12*(10), Article 2403. https://doi.org/10.3390/polym12102403

Tajvidi, M., & Takemura, A. (2010). Thermal degradation of natural fibre-reinforced polypropylene composites. *Journal of Thermoplastic Composite Materials*, *23*(3), 281–298. https://doi.org/10.1177/0892705709347063

Tharanathan, R. N. (2005). Starch - Value addition by modification. *Critical Reviews in Food Science and Nutrition*, *45*(5), 371–384. https://doi.org/10.1080/10408390590967702

Travalini, A. P., Lamsal, B., Magalhaes, W. L. E., & Demiate, I. M. (2019). Cassava starch films reinforced with lignocellulose nanofibers from cassava bagasse. *International Journal of Biological Macromolecules*, *139*, 1151–1161. https://doi.org/10.1016/j.ijbiomac.2019.08.115

Weerapoprasit, C., & Prachayawarakorn, J. (2019). Characterization and properties of biodegradable thermoplastic grafted starch films by different contents of methacrylic acid. *International Journal of Biological Macromolecules*, *123*, 657–663. https://doi.org/10.1016/j.ijbiomac.2018.11.083

Wollerdorfer, M., & Bader, H. (1998). Influence of natural fibres on the mechanical properties of biodegradable polymers. *Industrial Crops and Products*, *8*(2), 105–112. https://doi.org/10.1016/S0926-6690(97)10015-2

Yokesahachart, C., Yoksan, R., Khanoonkon, N., Mohanty, A. K., & Misra, M. (2021). Effect of jute fibres on morphological characteristics and properties of thermoplastic starch/biodegradable polyester blend. *Cellulose*, *28*(9), 5513–5530. https://doi.org/10.1007/s10570-021-03921-8

Zhang, Y., & Han, J. H. (2006). Plasticisation of pea starch films with monosaccharides and polyols. *Journal of Food Science*, *71*(6), 253–261. https://doi.org/10.1111/j.1750-3841.2006.00075.x

Zhang, Y., Rempel, C., & Liu, Q. (2014). Thermoplastic starch processing and characteristics: A review. *Critical Reviews in Food Science and Nutrition*, *54*(10), 1353–1370. https://doi.org/10.1080/10408398.2011.636156

Zullo, R., & Iannace, S. (2009). The effects of different starch sources and plasticizers on film blowing of thermoplastic starch: Correlation among process, elongational properties and macromolecular structure. *Carbohydrate Polymers*, *77*(2), 376–383. https://doi.org/10.1016/j.carbpol.2009.01.007